Summer 2023

Investigation of Defect Production and Displacement Energies in Wurtzite Aluminum Nitride

Sean Anderson
Missouri University of Science and Technology

Department:

INVESTIGATION OF DEFECT PRODUCTION AND DISPLACEMENT ENERGIES IN WURTZITE ALUMINUM NITRIDE

by

SEAN THOMAS ANDERSON

A THESIS

Presented to the Graduate Faculty of the

MISSOURI UNIVERSITY OF SCIENCE AND TECHNOLOGY

In Partial Fulfillment of the Requirements for the Degree

MASTER OF SCIENCE

in

PHYSICS

2023

Approved by:

Aleksandr Chernatynskiy
Joseph Graham
Halyna Hodovanets

ABSTRACT

Aluminum Nitride is an active element of sensors that monitor the performance and well-being of the nuclear reactors due to its piezoelectric properties. Yet, the variations of its properties under irradiation are largely unexplored. We report the results of the molecular dynamics simulations of the structural changes in AlN under irradiation via the knock-on atom technique. By creating and evolving the irradiation cascades due to energetic particle interaction with the atom of the crystalline lattice we determine the rate of the defect production as a function of the deposited energy. Further, we determine a displacement energy, a key characteristic that describes how efficient the defect production in the given material is. Comparison with the isostructural GaN is provided.

ACKNOWLEDGMENTS

I would firstly like to extend my utmost and most earnest gratitude for my advisor Dr. Aleksandry Chernatynskiy. Without his guidance, patience, and mentorship, the following work could never have come to fruition, and his direction helped me grow in my own understanding.

I would like to further thank my committee Dr. Joseph Graham and Dr. Halyna Hodovanets for their expertise, assistance, and time during the course of this research.

For the use of their computational clusters, I would like to thank the Missouri University of Science and Technology. And for constantly helping me push my knowledge and stimulating my intellectual growth, I would like to thank the Physics department and Faculty as well for their help.

To my friends, I extend my enduring appreciation over all my time spent here. Not only as peers in academia, to learn and realize my education with. But also as reliable support, as people to trust and confide in.

Finally, to my parents and my family: your unconditional and endless love and support has helped me become who I am today. Words could never possibly be enough to express my gratefulness to you, and my endless thankfulness towards you.

TABLE OF CONTENTS

Page

LIST OF ILLUSTRATIONS

LIST OF TABLES

1. INTRODUCTION

Acoustic and/or ultrasonic measurement techniques have been identified as a promising methods for measuring temperature, pressures, liquid flows and possibly other parameters in the advanced nuclear reactors.[1] Advantages of this method include a possibility for more convenient measurements in opaque media, such as liquid metals. The ability for sound waves to travel through these mediums means that there is no need to create specialized ports for other measurement devices to enter through.

The physical process that these measurements seek to take advantage of to function is known as the *piezoelectric effect*. The piezoelectric effect is a well known property of certain materials that lack inversion symmetry, where applying stress or pressure to the material creates an electrical charge. This property is also dependent on various other parameters of the material as well. Critically, the materials dependence on temperature and it's internal structure.

The *Curie temperature* is the temperature at which a materials loses it's piezoelectric properties. Unfortunately, materials with large piezoelectric coefficients are typically ferroelectric compounds with a relatively low Curie temperature (about 600 K[2]), which limits their applications in the high-temperature, high-radiation environment of the nuclear reactors. This prompted a research focus on nitride compounds which feature non-centrosymmetric structure and piezoelectricity at temperatures up to their melting point, but with much lower piezoelectric coefficients. Acoustic surface waves techniques are currently in active development to mitigate the latter issue.

Furthermore, defects have long been known to play a role in the electronic properties of materials. While the beneficial and/or undesirable effects of any given defect is generally a case by case basis, what is clear is that even a small number of defects can create very large variations in a material. So a baseline knowledge of defect accumulation in these materials is very beneficial as a position to begin with.

Under these limitations, nitride ceramics are considered as a structural material for advanced reactors. Unfortunately, the irradiation resistance and defect accumulation of AlN has not been extensively studied so far, and here we present the results of simulations of threshold displacement energy, defect energetics and defect production under irradiation via the molecular dynamics simulations. Experimentally, there are a number of recent works devoted to the irradiation resistance of AlN as irradiated by He-ions[3, 4, 5, 6], heavy ions[7, 8, 9, 10], and neutrons[11, 12, 13].

The overall conclusion from these studies is that AlN shows higher radiation resistance than isostructural, highly studied GaN[14]. In particular, it is much more difficult to completely amorphize AlN [7, 8] and lattice constants remain nearly constants in response to irradiation [13]. The main mode of defect accumulations from these studies appear to be a formation of the dislocation loops in the basal plane,[11] but in much lesser amount than GaN.

Molecular dynamics (MD) is a successful methodology for the investigation of the radiation damage.[15] For AlN, it has been applied so far only on the basis of the ab initio calculations for the interatomic interactions. [16] These calculations, while rigorous, are also time-consuming and limited by relatively small simulations cell. For example, Xi and coworkers [16] simulated only the threshold displacement energy and only for a handful of crystallographic directions. Even for this few directions they found large variations of the displacement energy, ranging from 19 eV to 122 eV, indicating an importance of the careful averaging over multiple directions.

Nevertheless these calculations are a very important reference point for more expanded calculations using classical potentials presented in this work. Other nitrides have been investigated more thoroughly by MD, namely displacement energy, defect production, temperature effect in GaN all have been a subject of attention.[17, 18] This precedent work has already established some properties relating defect production and external factors, such

at He et al. found a weak dependence of irradiation effects on temperature, and Nord et al. investigating threshold displacement energies based on how the irradiated atom strikes the crystal.

This work will begin with an overview of molecular dynamics as a method of experimentation. We will discuss the conceptual underpinning of how these simulations correspond to observable results, and mention it's relevance to the current state of physics. We then explain it's application to the relevant questions, and how we use it to generate analyzable data. We then present our results for defect formation energies, displacement energies, and cascade productions for relevant potentials. We conclude in the final section and discuss potential interpretations of our analysis.

2. METHODOLOGY

2.1. MOLECULAR DYNAMICS

Theoretical models that can be built to solve problems and make predictions are very often handicapped by an unwieldy amount of mathematical complexity. But, with the advent of more efficient and powerful computer software and hardware, applications of computer simulations to relevant physics problems can be seen as a possible alternative solution to this issue. These computer simulations are an important scientific tool in modern physics as they allow testability of problems that are impractical to implement in a physical experiment, but also too unwieldy to calculate theoretically. In this way, computational physics can be seen as a ”bridge” between the experimental and theoretical sides of physics.

Molecular Dynamics is a class of these simulations that is focused on analyzing the movements and dynamics of a system of particles/atoms. As a general overview, molecular dynamics evolves a system of particles by discretizing Newton's Law of motion in time, and numerically solving for the trajectory of every atom. Repeated applications of this idea creates a generic algorithm for molecular dynamics to follow: evaluate forces between particles in the system, use these forces to move particles and update their positions, use these positions to calculate new forces, repeat. Once trajectories of the atoms are known, the practitioner uses them to calculate any dynamic or static properties of interest. By the way of an example, by averaging the square of the velocity over the trajectories of all particles, one can calculate their average kinetic energy, and thus the temperature of the system.

2.2. LAMMPS

The outline of the algorithm discussed previously leaves itself open to many questions, cheif among them being creating software that can carry out these simulations. Thankfully, many open-source software are available to apply molecular dynamics, and

in this work, we have chosen to use the LAMMPS[19] package. The LAMMPS package is an extensively used software to perform molecular dynamics due to it's flexibility in calculating desired physical quantities for the practitioner, and a wide range of implemented interatomic potentials. Furthermore, of particular importance is it's native support of parallel processing, using Message Passing Interfacing for efficient calculations.

LAMMPS simulations are controlled from an external *input script* prepared by the researcher. Each line of this file starts by invoking a command that will give LAMMPS instructions to follow, and subsequent characters on this line are parameters for that command if any are required. This pattern is repeated until LAMMPS reaches the end of the external file, upon which it will close and be completed.

LAMMPS provides a large swathe of possible commands to use, but that is far more extensive than what this thesis allows. Instead, basic commands and a short description of them are provided in the subsections that follow. The focus of these will be placed on commands that have fundamental and defining effects on the evolution of the system. A full LAMMPS input script and an abridged explanation will be placed in the appendix at the end of this thesis as an example of these being used, and a glimpse at some of the commands not covered here.

2.2.1. Atomic Structure. The atomic structure for Wurtzite Aluminum-Nitrogen wurtzite (w-AlN) is shown in Figure 2.1 and is in the space group 186. It is part of the Hexagonal crystal family, with two hexagonal sublattices. Of particular importance is to note the lack of inversion symmetry in the crystal. Since the atoms dispersed in the unit cell are not equally spaced between either ends, there is a lack of symmetry about reversal. This gives rise to the piezoelectric properties of this structure, and warrants its consideration.

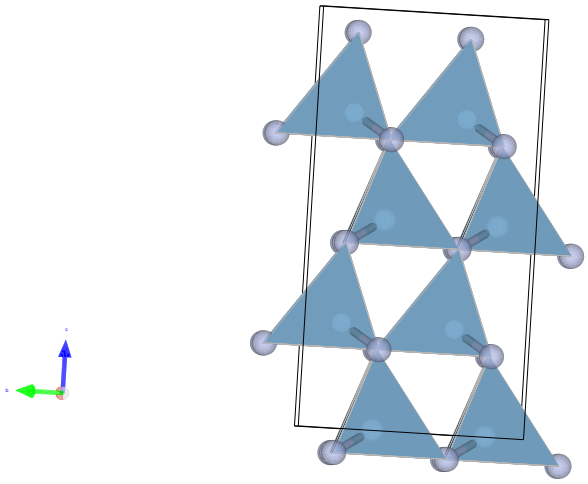

Figure 2.1. Unit cell for w-AlN replicated 2 by 2 where nitrogen are gray, and aluminum are in the polyhedra.

LAMMPS allows for multiple methods to create a lattice and place atoms on the sites. The *lattice* command is how LAMMPS creates a lattice for atoms to use. It has standard common lattices (square, face-centered, etc. etc.), but also has the option to create custom lattices. These custom lattices then use the *bases* and *create atoms* command to define lattice sites and what atoms will inhabit those spaces.

After a unit cell has been created via previous commands, the command *replicate* will repeated the desired amount of times in the x, y, z direction. This allows for an efficient creation of a supercell as the lattices and atoms will be created automatically, instead of having to manually declare all of them.

2.2.2. Timestep. The timestep of a simulation defines the length of time between subsequent calculations of forces acting on the particles. This number is equivalent to the timestep parameter in the Verlet Algorithm (see below).

Selection of a timestep balances two fundamental needs: Efficiency and Accuracy. A small timestep will yield more accurate results compared to a generically larger timestep. This is due to the more frequent force calculations and recalculation of trajectories which will

naturally lead to less errors being accumulated in the integration. However, the increased repetition of these calculations means that the computation hours required will increase. Choosing a small timestep is thus prioritizing accuracy over efficiency.

A large timestep will very much have inverse effects. Since each step occurs less frequently in time, the simulation will require fewer computations to be run. However, since the forces are not recalculated as often this will lead to an error-buildup in the trajectory. In the worst possible case scenario, the results from a simulation with a much too large timestep could have very little physical significance!

It's clear then that the choice of a timestep is both essential, and a balancing act. One naturally wants accurate results from their simulations, which leads itself to a smaller timestep. But if it is chosen to be far too small, then the small timestep will demand an incorrigible amount of computation hours in order to be simulated.

Both of these factors must be weighed when setting the timestep, and is generally decided upon by the physical characteristics of the system. If a system has a natural "characteristic time scale" (for example the period of a pendulum, or the period of a planets orbit), the timestep is generally set to some fraction of that time scale. For a solid state system, the caracteristic time scale is that of atomic motion in the potential created by the neighboring atoms and corresonds to the time scale of lattice vibrations, or phonons. Phonon frequency scale is $10THz = 10^{13}Hz$ and thus typical timestep for molecular dynamics of atomic scale is $1fs = 10^{-15}s$.

The quality of a timestep can also be evaluated by observing some fundamental property of the system. For instance, one could observe how well the total energy of the system is conserved at a given timestep. If the total energy is not conserved to a desirable degree, the timestep could be lowered for a more accurate simulation.

In LAMMPS, the timestep is declared with the command *timestep* followed by an integer.

```
1 timestep n
```

The units of n are decided by an earlier command called *units*, that has not been discussed here.

2.2.3. Thermostats. Thermostats are a fundamental part of how a molecular dynamics simulation is controlled, as it allows the researcher to exhibit control over various fundamental quantities of their system. In general, any given *thermostat* in a simulation will attempt to integrate Newton's Equations of Motion in a way that is consistent with some specified extenal parameter (or parameters), and a given value. An equivalent statement is that the trajectories created under certain thermostats are consistent with various statistical ensembles that one would be familiar with from statistical mechanics.

Different thermostats will require slightly different contributions to the Newton's equations of motion. For this reason, LAMMPS combines thermostats with the integrator of the equation of motion. The basic integration techniques remains the same for all thermostats: It is the standard and robust Stoermer-Verlet algorithm, prescibed by the following equations:

$$\mathbf{x}(t + \Delta t) = \mathbf{x}(t) + \mathbf{v}(t)\Delta t + \frac{1}{2}\mathbf{a}(t)\Delta t^2 \tag{2.1}$$

$$\mathbf{v}(t + \Delta t) = \mathbf{v}(t) + \frac{\mathbf{a}(t) + \mathbf{a}(t + \Delta t)}{2}\Delta t \tag{2.2}$$

This algorithm prescribes an iterative process to update the velocity ($\mathbf{v}$) and positions ($\mathbf{x}$) of particles in increments of a timestep Δt. A particles trajectory can be integrated for a single timestep by knowledge of it's position and velocity at time t. Firstly, the current position and velocity are used to calculate 2.1. At this new position $\mathbf{x}(t + \Delta t)$, the new acceleration is calculated from the interactions potentials with other atoms. Finally, the velocity is updated according to 2.2, which concludes one iteration of the algorithm.

The syntax to implement a thermostat is invoked via the use of a *fix* command.

```
1   fix ID atomGroup thermostat keywords
```

ID is the number ascribed to the thermostat for reference in future commands, and the *atomGroup* is what set of atoms the thermostat will be applied to. Some possible options for the *thermostat* options will be explained in the next sections, along with their function.

2.2.3.1. NVE. The NVE thermostat corresponds to the microcanonical ensemble from statistical mechanics. Trajectories under this thermostat will have a constant number of particles in the simulation, a fixed volume size, and a constant energy up to a precision of the calculations. This thermostat uses Stoermer-Verlet integration algorithm 2.1 without any modificiations.

2.2.3.2. NPT. The NPT ensemble corresponds to the isothermal-isobaric ensemble, a special case of canonical ensamble from statistical mechanics. Trajectories under this thermostat are characterized by the number of particles in the simulation, the target pressure, and the target temperature. By default, LAMMPS implements this thermostat by invoking specialized form of Nose-Hoover style integration algorithm. This algorithm adds fictitious forces to guarantee desired temperature on average.

2.2.4. Potentials. LAMMPS includes many pre-defined potentials that can be used to simulate the interaction between atoms. It further includes support for long-range interactions, additions of potentials, and combinations of potentials. Should one need more nuanced control over their potential, it supports loading interactions from external files that can be suited to the users needs.

A LAMMPS potential is defined by the command *pair_style*, with syntax as

```
1  pair_style potential potentialArgs
```

The *potential* keyword decides what potential interaction LAMMPS will use to make force calculations. The *potentialArgs* are specific keywords based on the chosen potential.

The motivation, conceptual understanding of, and discussion of chosen potentials is of such import though, that an in-depth explanation will be split into it's own section.

2.3. DEFECTS

An ideal crystalline solid structure is charactarized by a periodically repeating pattern of atoms known as a unit cell. This pattern is regular at fixed distances, and should be the same at all points. However, when an atom receives enough energy, it is possible for it to break this regularity, and wander elsewhere in the crystal. Any interruption of the repeating pattern in this manner is what's known as a *defect*, and is what we will concern ourselves with for the following sections.

When an atom breaks the regularity in this fashion, it will find a local minima somewhere else in the solid and create an *interstitial*. In this case, the atom has come to rest and settled down in an intermolecular space in the crystal. It is worth stressing that this new location the atom will settle into will not be on *any* ideal lattice point, it's own or otherwise.

After careful thought of the interstitial, one may stumble upon a reasonable followup question: if an atom has left it's position on the lattice and been displaced somewhere else, what of where it originally resided? Certainly, the atom that is now in an interstitial location naturally cannot be occupying the ideal lattice site it was before. And this "hole" that left behind is itself an irregularity in the crystal structure! The name for this hole where the atom was residing, but no longer occupies is called a *vacancy*, and is defined as any site that has no atoms occupying it.

Note how the above definition of an interstitial and vacancy seem to go hand in hand with each other. After all, in order to create an interstitial, an atom certainly has to be displaced away from it's site. And as was just explained, this by definition will create a vacancy. interstitial-Vacancy pairs created in this manner are referred to as *Frenkel Pairs*, and are dominant when the total number of atoms must remain a constant.

Now there may be a case where two atoms of differing species are simultaneously kicked out of their sites, become interstitials, and then come to rest again in the vacancy the other atom left behind. This "swapping" of atoms is specifically known as an *antisite*,

and in effect occurs when a location on the lattice is occupied by the different type of atom. Note that in the above example, if the two atoms are of the same species, no antisite is created. This is because in the final structure, the correct species of atom still ends up on the correct lattice site.

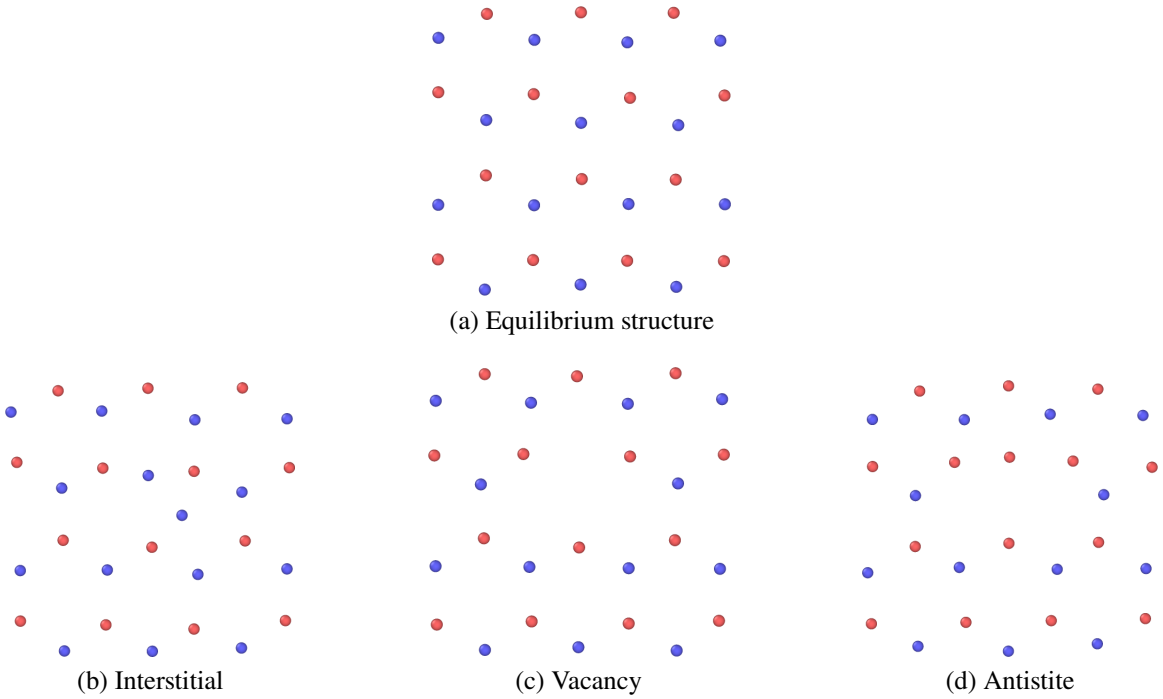

(a) Equilibrium structure

(b) Interstitial (c) Vacancy (d) Antistite

Figure 2.2. Comparison of discussed defects and the equilibrium structure.

In Figure 2.2 we have shown comparisons between the 3 defect types discussed, and shown the equilibrium structure for comparison. The atoms are shown in the xy-plane, and all atoms that are not on the same plane have been removed for clarity.

2.3.1. Wigner-Seitz Analysis. In order to implement the above qualitative definitions, we need some mathematical machinery to quantitatively analyze it. To this extent, we will apply the use of what is known as Wigner-Seitz cells. A single Wigner-Seitz cell is defined as the locus of all points around a lattice site that are closer to it than any other lattice site[1]. When this is applied to every atom in a system, you divide the entire volume of the

[1]For those familiar, this is a particular application of what is known as Voronoi Decomposition

system into these Wigner-Seitz sites. Of special note is that, by definition, a Wigner-Seitz cell constructed in this manner will always have *one and only one* lattice point inside of it. This property is what allows us to quantitatively measure defects and interstitials.

First, a Wigner-Seitz cell for every atom is calculated and constructed from an equilibriated position. Then, after some interactions, the atoms in the cell are translated, interact with each other, and are otherwise displaced into a new configuartion. Comparing this new configuration of atoms to the original Wigner-Seitz map allows us the desired ability to count interstitials and vacancies. Any site that has two or more atoms located in it are counted as interstitials. Conversely, any cell that has no atoms is counted as a vacancy.

Antisites, unforrunately, cannot be detected with this simple counting scheme. Since antisites still only have one atom occupying a site, simply counting the number of atoms there yields them indistinguishable from a normal site. In order for these to be recognized, the original Wigner-Seitz map not only needs a count of atoms, but also the *species* of atoms currently occupying it, and the type of site it was at equilibrium. With this extra information though, antisites can be calculated relatively simply. Instead of counting the number of atoms in a site, they are found by comparing the site type of the lattice point to the type of atom currently occupying it. If the type of the atom does not match the type of the site, and it is the only one occupying it, it is an antisite.

This process of constructing Wigner-Seitz Cells, tracking the trajectory of the motions of the particles, and counting the interstitials, vacancies, and antisites, was implemented with a program called OVITO [20]. Ovito is a program that allows us to visualize data output from LAMMPS (or other Molecular Dynamics packages) and visualize and analyze it in various facets. Of most import to us though, is it's built in support for the above Wigner-Seitz construction, and antisite detection. In addition to it's native visualization of LAMMPS output, it also features a free Python module for efficient scripts to analyze

outputs. This was the main method utilized to analyze our results. A python script was created (listed in the appendix) to count the maximum number of each defect, the average number of each defect at the end of the simulation, and average these results.

2.3.2. Defect Formation Energy. A *Defect Formation Energy* is defined as the energy difference between that of a crystal with exactly one defect and that of ideal crystal. These energies play a very large role in determining the production and evolution of defects in the crystal, as they will control how energetically demanding it is to create defects in the crystal. It should make sense, and has been shown before, that the quantity of defects in a crystal will be proportional and very closely related to the defect formation energies. Any defect that has a low formation energy will be more likely to appear, and conversely, any defect with a higher formation energy will be less likely to appear.

In this work, we calculate the formation energies of the defects described in Section 2.3. This will in total, give us 3 energies to calculate: The energy of an aluminum interstitial-aluminum vacancy pair, the energy of a nirogen interstitial-nitrogen vacancy, and a synchronous pair of aluminum-nitrogen antisites. Note, that due to the constraints of the interatomic potential, we cannot calculate formation energies of the individual interstitial or vacancy, but only that of the Frenkel pair. Comparisons of the energies of the systems with different number of atoms, which is required for an individual interstital or vacancy, is only possible if the reference state energy of the removed/added atom, i.e. it's chemical potential, can be calculated. For the vast majority of the classical potentials this is impossible, and thus energies between two systems can only be compared if the total number of atoms is the same.

An aluminum Frenkel pair is defined as *any* site that has two aluminum atoms in it, or a nitrogen site that has a nitrogen and aluminum atom occupying it. Calculating this quantity involves beginning with the ideal lattice structure and displacing one aluminum atom some distance away from it's equilibrium position. This displacement was not short enough that it would interact with it's original vacancy, nor long enough that it could do the

same via periodic boundary conditions. After this displacement occurred, the energy of the system was minimized with respect to ionic positions. The difference between the energy of the original system, and the newly minimized system was defined as the aluminum Frenkel pair energy. A nitrogen Frenkel pair is defined as *any* site that has two nitrogen atoms in it, or an aluminum site that has an aluminum and nitrogen atom occupying it. This quantity was calculated in much the same way as the aluminum Frenkel pair, with the same outline. The same consideration was given to the magnitude of the displacement.

An antisite is either an aluminum site with only a nitrogen atom occupying it, or a nitrogen site with only an aluminum atom occupying it. This quantity was calculated by directly swapping the two coordinates of the aluminum and nitrogen atom that had been moved previously. Note that this direct swapping of coordinates does not create any interstitials, and is only a pure antisite. The vacancy that would have been created by either of the two atoms being displaced is replaced by the other moving to it's location. With only a pure antisite in the crystal, the same energy minimization required, and the difference in energy was defined as the antisite defect formation energy.

Note that the above defintions restrict our view to only sites that have at most two atoms in them, as in the case of Frenkel pairs. Note that is is possible to have more than three atoms occupying a site during an irradiation cascade, although these are seen as more complicated defect clusters, and will not be expounded upon in this work.

2.3.3. Displacement Energy. In an irradiation cascade, the the lowest amount of kinetic energy given to one particular atom that causes defects to form is known as the *Displacement Energy*. This quantity is more relevant to the defect production in a cascade since it also takes into account the kinetic barrier that atom needs to overcome in order to settle into a local minimum atomic configuration that represents a defective structure. For this reason, the magnitude of the displacement energy is typically greater than the defect formation energy due to this extra required energy.

However, the defect formation energy as described is calculated for well-separated individual defects and does not take the defects interaction in the account. The Frenkel pair however, will have different formation energy depending on the vacancy-interstitial pair separation. For this reason it is also possible to have displacement energy smaller than the defect formation energy, if the resutant defects are formed near each other.

More considerations must be made when defining the displacement energy however. This definition of the displacement energy introduces multiple dependencies that can change when a defect could or could not be created. For this work, we will account for differences in displacement energy arising from initial positions and direction dependence, and make a minor note of the expected behavior of this value.

For atoms of a low knock-on energy that we expect to be simulating, it is unlikely for the atom to travel far away from it's original site and will only interact with it's local neighbors. Furthermore, because it has such a low energy, minor variations it may experience in the kinetic barrier could play a large role in whether or not a defect is produced. With this in mind the environment immediately surrounding the atom that will be displaced can have a significant effect on what energies may or may not create a defect. Slight variations in an equilibrium position can shift the kinetic barriers shape just enough that it may allow a lower energy knock on atom to pass and create an intersitial.

Similarly to the environment around the atoms, there is also a potential difference that can arise from what direction the atom is sent in. If the crystal structure has any significant anisotropy in it's structure, two different trajectories could feel significantly different kinetic barriers. Similar reasoning means that one can expect different displacement energies based on the direction the atom is sent in as well.

With these two being considered, we expect the displacement energy to behave roughly as a step function. Once an atom has enough energy to create a defect, adding extra energy to the particle should, in theory at least, only allow it more momentum to deposit into the system. This is not exact though. It is possible that with extra momentum even

after creating the defect it is possible for the atoms to anneal back to it's previous vacancy position and remove the defect it created. It is therefore possible to sometimes see an energy higher than the displacement energy fail to create a lasting defect.

By way of these two considerations, it's clear that displacement energy becomes a statistical quantity that can have variations, rather than a single consistent result. This is something we will account for in our analysis of the displacement energy.

2.4. PRIMARY KNOCK-ON ATOM

In order to investigate the irradiation cascade, the *Primary Knock-on Atom* (PKA) technique was employed[21]. In a PKA simulation, a given atom is chosen to serve the role of an "irradiated" particle. To this end, it is given a specified incoming energy and allowed to impact the system, and begin to transfer it's momentum into the crystal. The subsequent dynamics and trajectory of the crystal is monitored and tracked as the molecular dynamics simulation is run.

This technique will split our simulation up to 3 distinct phases: Equilibration, Irradiation, and Annealing. Our simulations for these cascades consisted of 640,000 atoms in an 155.5 Angstrom x 215.46 Angstrom x 199.19 Angstrom box. Before the simulations began, the atoms were energetically minimized to a local minimum.

2.4.1. Equilibration. To begin the simulations one ought to specify position and velocity of every atoms in the system. While the positions are those that correspond to the ideal lattice sites, velocities are drawn from the Maxwell-Bolzmann distribution with the desired temperature. These initial conditions, however, do not correspond to the atomic system in the equilibrium, and it is not the most likely microstate. When initialized in this manner, all atoms at this moment are at their ideal lattice positions, something that is exceedingly unlikely. Thus every simulation begins with the equilibration stage, when it is subject to the NPT thermostat. Fixing the pressure allows the crystal to adjust its volume to that appropriate for the desired temperature, when taking into account thermal

expansion. The temperature and its fluctuations are monitored, and once the themperature is stabilized at the desired temperature with the fluctuations appropriate for our system size, we declared the system to be in equilibrium. For AlN at room temperature we reach satisfactory equilibrium in about 10 ps of simulated time.

To estimate the statistical variations in the defect production upon irradiation we have created 5 different realizations by letting them run for different amounts of time at the equilibration stage. They were run for 20,000 timesteps (20 ps), 21,000 timesteps (21 ps), 22,000 timesteps (22 ps), 23,000 timesteps (23 ps), and 24,000 timesteps (24 ps). The final structures of these runs were recorded and were used as the beginning points for the next phases of simulation. The equilibration was run at a constant timestep of 0.001 ps. The controlling thermostat was NPT at temperature of 300 K and pressure of 0 Pa.

2.4.2. Irradiation. The irradiation phase of the simulation starts with choosing a nitrogen atom at the bottom-center face of the cube and giving it a velocity corresponding to the chosen PKA energy. The thermostat is changed to the NVE thermostat at this point, in order to eliminate the influence of the thermostat on the dynamics of the system. This is due to the PKA atom having kinetic energy substantially greater than the average kinetic energy. This amount of additional kinetic energy is sufficiently large to change the overall temperature of the system. At 10 keV, the additional energy of the system was enough to increase the temperature by 50 K, although lower energies had negligible changes to the temperature. It is worth noting that any temperature dependence on cascade production has been investigated on a much wider scale before on GaN. The work done there however suggests that there is very little dependence on temperature for cascade productions, so we can safely assume the same here.

This phase of the simulation runs for a shorter time for only a maximum of 0.5 ps, and at a smaller timestep. The exact value of the timestep varies, but was smaller for higher energies. It was always set such that the total energy of the system never varied by more than 100 eV over the simulation run. This accuracy is sufficient when compared with

other energy scales in the system: the kinetic energy of the PKA is changing in 1 keV-10 keV interval, thus the MD energy drift is of 1-10% of this value. The total energy of the system is even greater (on the scale of 10^6 eV) than that and thus, this level of accuracy is sufficient. Finally, upon careful analysis of the trajectories, we found that the largest variations in the total energies happen during the head-on collisions in this phase of the simulation. In this phase,atoms are entering the regions of the largest forces, and the energy drift will be substantially smaller for the rest of the evolution. It is during this part of the cascade simulation that we expect to find the most defects produced. This is due to the large influx of energy deposited into the system still causing atoms to collide and displace other atoms as the energy is dissipated.

2.4.3. Annealing. The last part of the simulation is the annealing phase. This phase was run at a larger timestep than the irradiation phase due to the less energetic atoms present in the simulation. The annealing phase was run as one simulation until it reached a final time of 2 ps. This ending structure was seen as the end structure, and is what is analyzed for defects.

With the knock-on atom having dissipated most of it's energy into the system, it begins to re-equilibrate and settle into a new minimum. During this phase, many of the interstitials that were created during the irradiation phase will annihilate with vacancies. The atoms still carry enough energy to undo a jump from an interstitial position to a nearby vacancy, thus annealing out a defect.

Many of the defects in the system will anneal out relatively quickly, but a certain portion of those defects will be long lasting. In theory, even these long lasting defects could eventually anneal away, on the time-scales associated with the defect migration times. However, in the realistic irradiation experiment, there is a flux of the irradiation particles and annealing of the defects will compete with new defects production from the upcoming particles. For this reason, the amount of these long-lived defects generated by the individual knock-on atom is a relevant quantity to access the radiation damage in a particular material.

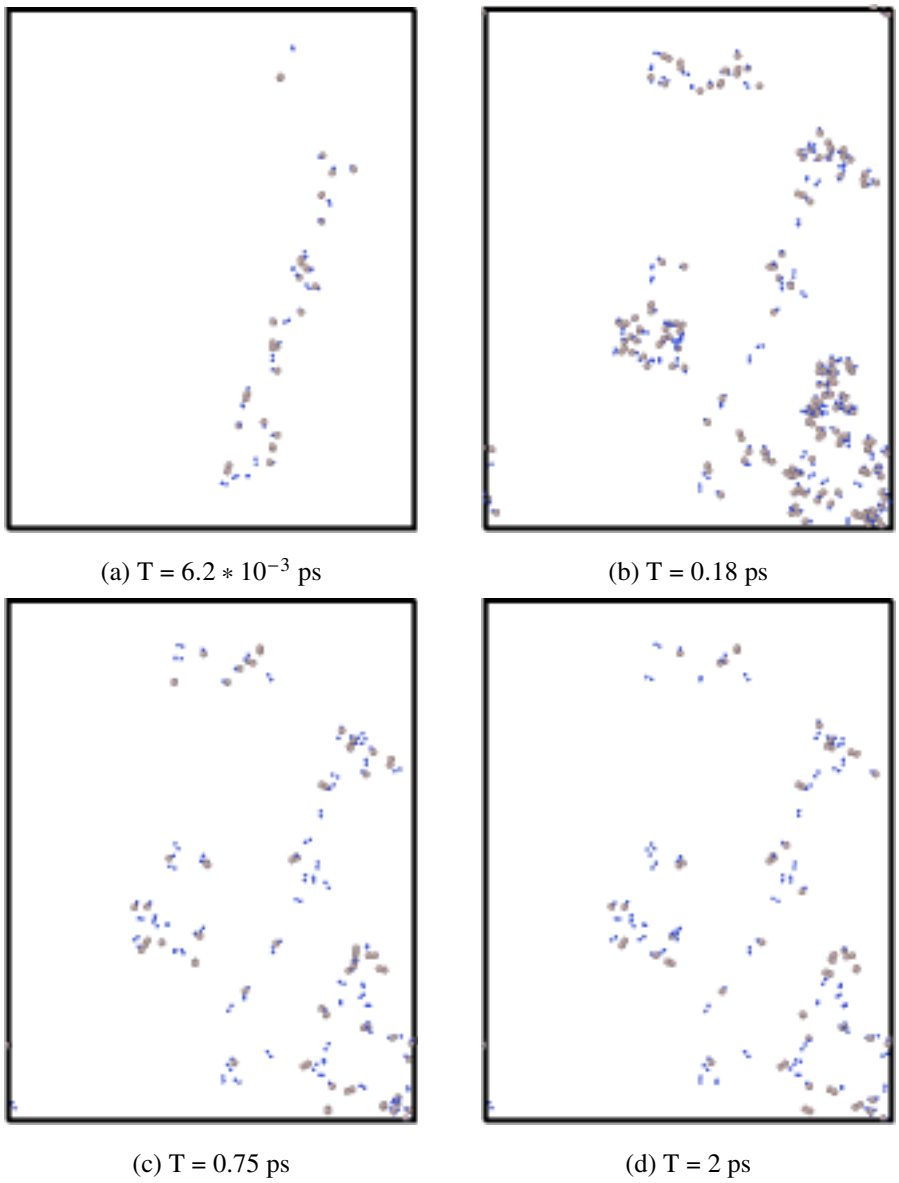

(a) T = $6.2 * 10^{-3}$ ps

(b) T = 0.18 ps

(c) T = 0.75 ps

(d) T = 2 ps

Figure 2.3. A sampling of the crystal defects at various points in time

.

A typical example of the radiation cascade from our simulations is shown in Figure 2.3. For clarity, only the defective atoms are shown at the different moments of the simulations. One can see the quick development of the defects in the initial stage. The second frame corresponds to the maximum defects generated before the subsequent annealing. The

last two frames are nearly identical, indicating that further evolution will happen on much longer time scales. For verification purposes we ran a few simulations up to 10 ps and no further changes were detected.

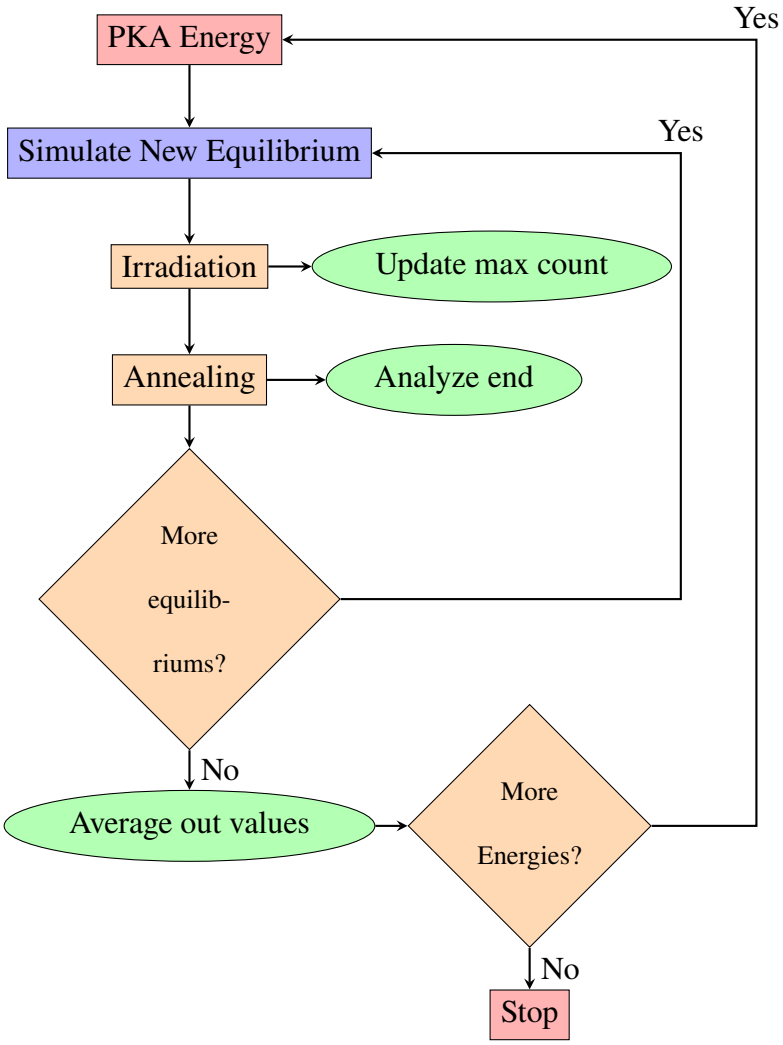

Figure 2.4. Flowchart for PKA simulations

2.4.4. PD and NRT Models. There are a number of theoretical models that can be used to predict the extent of defect productions in a crystal after a PKA event. Kinchin and Pearse (KP) [22] suggested a model based off of hard sphere collisions, where any atom with an energy greater than the average displacement energy (E_d) would create a displacement. Further, any atom with an energy $> 2E_d$ can not only create a displacement itself, but the atom it collides with can also create a displacement. Based on this assumption, the KP

model suggests the number of displacements formed N follows a linear form dependent on the displacement energy E_d, and the energy of the PKA atom E:

$$N_d = \begin{cases} 0 & 0 \leq E \leq E_d \\ 1 & E_d \leq E \leq 2E_d \\ \frac{E}{2E_d} & E \geq 2E_d \end{cases} \tag{2.3}$$

Norgett, Robinson, and Torrens [23] refined this model by taking into account the energy lost in that not all of the energy of an atom can go towards creating defects. Some of the knock-on energy E will be lost to electronic stopping power, so that the available energy to create defects is $\tilde{E} < E$. Furthermore, simulations performed by NRT showed that some 20% of initial displacements will be refilled by another atom (note that this process is NOT the long lasting recrystallization discussed in 2.4.3). This motivates further a prefactor of 0.8 be multipled to the KP model. The resulting NRT equation appears as such:

$$N_d = \begin{cases} 0 & \tilde{E} < E_d \\ 1 & E_d < \tilde{E} < 2E_d \\ \frac{0.8\tilde{E}}{2E_d} & 2E_d < \tilde{E} \end{cases} \tag{2.4}$$

It is worth noting that neither 2.3 and 2.4 account for long term annealing from recrystallization. This can be taken into account however by considering how efficient defects are able to anneal out. Defect annealing can be modelled by taking N_d and multiplying it by some factor $\Phi < 1$.

3. POTENTIALS

The choice of any interatomic potential is of the utmost importance when concerned with any molecular dynamics simulation. The choice of an interatomic potential will define how particles interact with each other, and so will largely define the results of the simulation.

AlN is a well-studied material, and has had many potentials[24, 25] developed for it over recent years of work. Xiang et al. compared molecular dynamics simulations between 3 recently proposed variants of aluminum-nitride potential: the Tersoff potential[26] with parameters developed by Tungare et al.[27], the Vashista potential[28, 29] suggested by Vashista et al., and the Comb3[30] potential proposed by Liang et al. While many more potentials are discussed in this paper, only the 3 mentioned were modelled for results. Unfortunately the modelled potentials were not analyzed for specific properties that are relevant for a PKA simulation. So while we were able to look at this for overall guidance, it did not provide a simple answer for a question of which potential is the most suitable.

In light of this we used the bond-order Tersoff potential the paper suggested on account of it's fast computational time. We also applied the Buckingham potential due to previous familiarity with it, and established use in molecular dynamics simulations.

Both of these potential styles have been applied with success to recreate basic properties expected of Aluminum-Nitride[27, 31] as AlN exhibits properties suited for both of them. The Buckingham potential lacks any specified directionality in it's interaction potential (as we will see) which is suitable for ionic compounds. Tersoff, being a bond-order potential, does have specified dependence on directionality in it's potential which is normally applied for modelling of the covalent materials. As AlN has features of both of these, they both might be suitable descriptions.

Table 3.1. Parameters used for the Buckingham Potential

	A (eV)	ρ (Å)	C (Å^6 eV)	Z_i	Z_j	r_c (Å)
Al-Al	5131.167	0.3040	248.0	13	13	16
Al-N	698.547	0.3224	0.0	13	7	16
N-N	5134.176	0.3140	283.8	7	7	16

3.1. BUCKINGHAM POTENTIAL

The Buckingham potential is a 2-body potential that is used to model a potential with an exponential repulsive part, and a r^{-6} attractive part. Additionally, we add on the familiar coulombic potential term to model the long range behavior.

$$E_{ij} = A \exp\left(-\frac{r_{ij}}{\rho}\right) - \frac{C}{r_{ij}^6} + \frac{Z_i Z_j}{4\pi\epsilon_0 r_{ij}} \quad r_{ij} < r_c \tag{3.1}$$

A is a constant term in energy units, ρ is a strictly positive constant in units of distance, and C is a constant term in units of Energy-Distanceˆ6. Z_i and Z_j denote the atomic number of the two atoms ($Z_{Al} = 13$, $Z_N = 7$) and r_{ij} is the distance between the two atoms. Table 3.1 summarizes the parameters used in the Buckingham potential for Aluminum wurtzite.

The positive exponential models repulsion between two atoms that arises due to the overlapping of their outer electron shells. The r^{-6} term models attractive forces between two atoms at longer range due to the London Dispersion Forces. The Coulombic force is well known, and is added to create a more accurate model for ionic crystals.

While the equation as written provides a good description of the interaction of atoms at a range near or longer than their energetic minimum, special care must be taken care if the separation can ever become too small. This is due to the attractive term r^{-6} diverging to negative infinity, causing the potential as a whole to diverge as well. The repulsive

exponential converges to the constant A at 0, and the Coulombic interaction diverges to infinity, but at a slower rate . Thus, at separations near 0, the Buckingham potential has an unphysical attraction between the two atoms that must be considered.

In order to accurately model the behaviors between atoms at separations near 0, we use the Ziegler-Biersack-Littmark (ZBL)[32] potential. The ZBL potential is a potential made to describe interactions between particles at very close separations, where the interaction can be described as purely Coulombic. The ZBL potential is given as

$$\begin{aligned} E_{ij}^{ZBL} &= \frac{1}{4\pi\epsilon_0}\frac{Z_i Z_j e^2}{r_{ij}^2}\phi\left(\frac{r_{ij}}{a}\right) + S(r_{ij}) \\ a &= \frac{0.46850}{Z_i^{0.23} + Z_j^{0.23}} \end{aligned} \tag{3.2}$$

, where ϕ is a screening function

$$\phi(x) = 0.18175e^{-3.19980x} + 0.50986e^{-0.94229x} + 0.28022e^{-0.40290x} + 0.02817e^{-0.20162x} \tag{3.3}$$

, and S is a switching function between an inner cutoff r_1 and outer cutoff r_c,

$$\begin{aligned} S(r_{ij}) &= C \quad r_{ij} < r_1 \\ S(r_{ij}) &= \frac{A}{3}(r - r_1)^3 + \frac{B}{4}(r - r_1)^4 + C \quad r_1 < r_{ij} < r_c \end{aligned} \tag{3.4}$$

where A, B, and C are all constants computed to ensure that the switching function smoothly ramps the energy and force to 0.

The ZBL potential can accurately model close separations between particles, and the Buckingham potential can accurately model long range potential, the two potentials must be joined together to create a coherent modelling potential. The ATSIM [33] library is a Python module that can smoothly create splines between potentials, and output the result in a form suitable for LAMMPS to read.

Table 3.2 summarizes the cutoff parameters chosen to create a splined potential.

Table 3.2. Spline parameters used to smoothly transition between ZBL and Buckingham

	r_1 (Å)	r_2 (Å)
Al-Al	1.0	1.4
Al-N	0.5	1.4
N-N	0.5	1.6

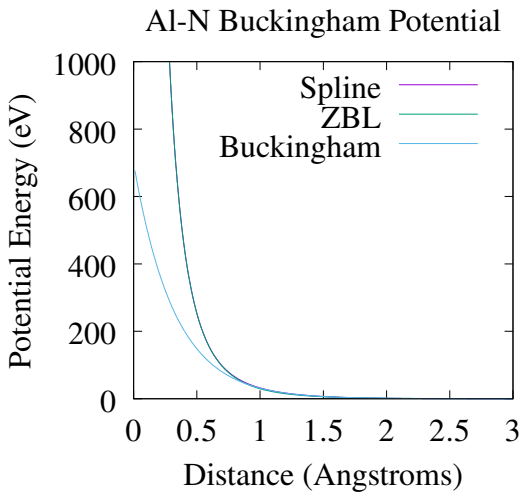

(a) Pairwise Buckingham potential between Aluminum and Nitrogen

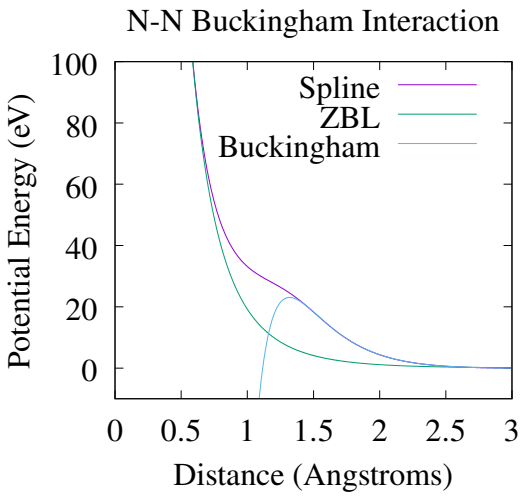

(b) Pairwise Buckingham potential between Nitrogen and Nitrogen

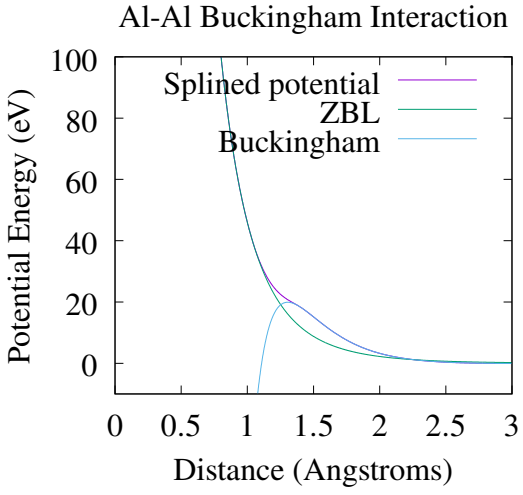

(c) Pairwise Buckingham potential between Aluminum and Aluminum

Figure 3.1. Graphs of the interaction potential for Buckingham, ZBL, and the spline

3.2. TERSOFF POTENTIAL

As opposed to the Buckingham potential that is a 2-body potential, the Tersoff potential[26] is a bond-order potential that includes pairwise interactions, and a bond-order potential that has a strength based on the environment around it. Furthermore, LAMMPS has a native modification that allows for the ZBL potential to be implemented at close ranges. While Tersoff potential does not feature the divergence for small interatomic separations, it nevertheless requires ZBL addition in order to be a sensible description of the interactions in these regions, as those will inevitably arise in irradiation modelling. The Tersoff Potential can be written as

$$
\begin{aligned}
E &= \frac{1}{2}\sum_i \sum_{j\neq i} V_{ij} \\
V_{ij} &= f_C(r_{ij})[f_R(r_{ij}) + b_{ij} f_A(r_{ij})] \\
f_C(r_{ij}) &= \begin{cases} 1 & r < D \\ \frac{1}{2} - \frac{1}{2}\sin\left(\frac{\pi}{2}\frac{r-R}{D}\right) & R - D < r < R + D \\ 0 & r > D \end{cases} \\
f_R(r) &= A\exp(-\lambda_1 r) \\
f_A(r) &= -B\exp(-\lambda_2 r) \\
b_{ij} &= (1 + \beta^n \zeta_{ij}^n)^{-\frac{1}{2n}} \\
\zeta_{ij} &= \sum_{k\neq i,j} f_C(r_{ik}) g[\theta_{ijk}(r_{ij}, r_{jk})] \exp\left[\lambda_3^m (r_{ij} - r_{ik})^m\right] \\
g(\theta) &= \gamma_{ijk}\left(1 + \frac{c^2}{d^2} - \frac{c^2}{[d^2 + (\cos(\theta) - \cos(\theta_0)]^2}\right)
\end{aligned}
\tag{3.5}
$$

In the above formula, f_R and f_A both represent independent pairiwse potentials, where one is repulsive and the other is attractive respectively. f_C is a function used to implement a cutoff range for the potential. Instead of choosing a distance r for which all potentials will be 0, f_C smoothly decreases from one to zero. This decrease starts at R, and the rate at which it decreases is determined by the parameter D.

b_{ij} is the bond-order feature of this potential, as it's strength is determined by the 3-body interactions around it. From quantum mechanical considerations, it is a monotonically decreasing function with respect to the number of atoms that have bonded with it (it's *coordination number*). The full considerations of this function are beyond this paper, but we will make note of the critical features of it. ζ is responsible for counting the number of bonds formed with an atom, and thus implements the monotonically decreasing behavior we ask for. The directionality in the potential is accounted for by g, where θ_{ijk} is the angle between two different bonds to an atom. You can see that the difference of cosines in the last term of g will minimize the potential energy of the bonds when they are near the optimum angle θ_0.

Further, LAMMPS allows a built in method for implementing the ZBL potenetial as a close range modifier. It has the same dependence on atomic numbers Z_i, Z_j, but also has parameter for a place to being the transition from ZBL to Tersoff r_c and how sharp that transition should be d_c. The qualitative behavior of these two parameters is identical in function to those of R and D, so the similar choice of variable names is chosen to highlight this.

Table 3.3 summarizes the parameters used[27] for the Tersoff potential. Any parameters that are not given a unit are imminently unitless.

Table 3.3. Parameters used for Tersoff potential model

	Al-Al	Al-N	N-N
m	3.0	3.0	1.0
γ	0.0	1.0	1.0
λ_3 ($\mathring{A}^{-1}$)	1.5	0.0	0.0
c	0.0748	0.178493	100,390
d	19.5691	0.20172	16.217
$\cos(\theta_0)$	-0.6593	0.045238	-0.5980
n	6.0865	1.0	0.72
β	0.3168	0.766120	0.0000011
λ_2 ($\mathring{A}^{-1}$)	0.927415234	2.38426	1.860592549
B (eV)	23.02954942	423.769	257.3159264
R ($\mathring{A}$)	2.7	2.20	2.34
D ($\mathring{A}$)	0.1	0.20	0.15
λ_1 ($\mathring{A}^{-1}$)	2.58526	3.557799	3.21305
A (eV)	492.674645	1044.77	1847.752014
Z_i	13	13	7
Z_j	13	7	7
r_c	1.3	0.7	0.95
d_c	10.986	21.9722	4.882

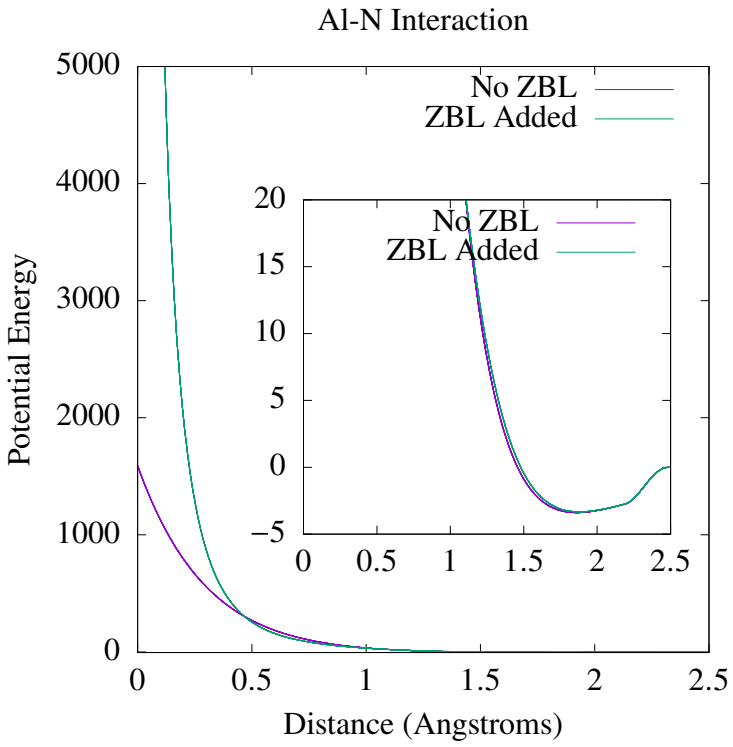

Figure 3.2. Tersoff-ZBL Potential for Aluminum-Nitrogen

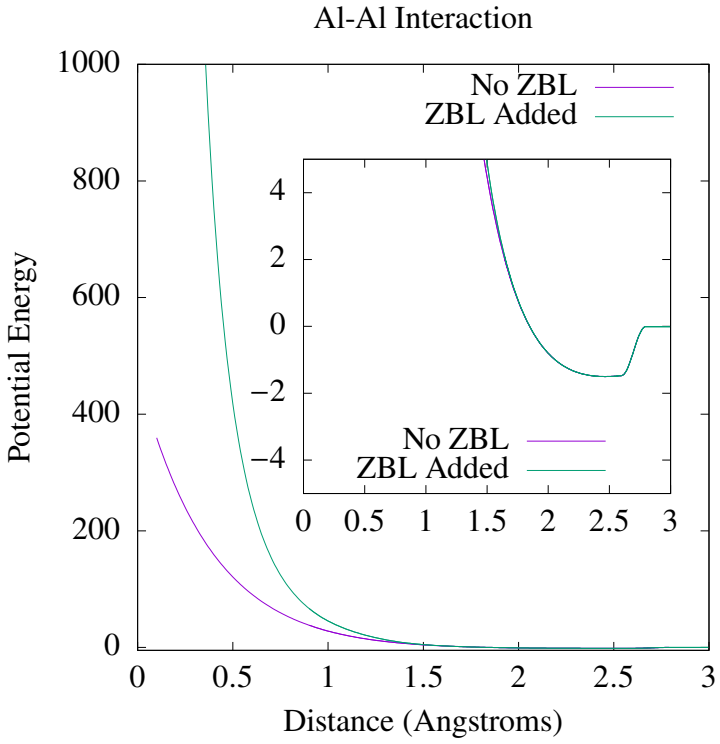

Figure 3.3. Tersoff-ZBL Potential for Aluminum-Aluminum

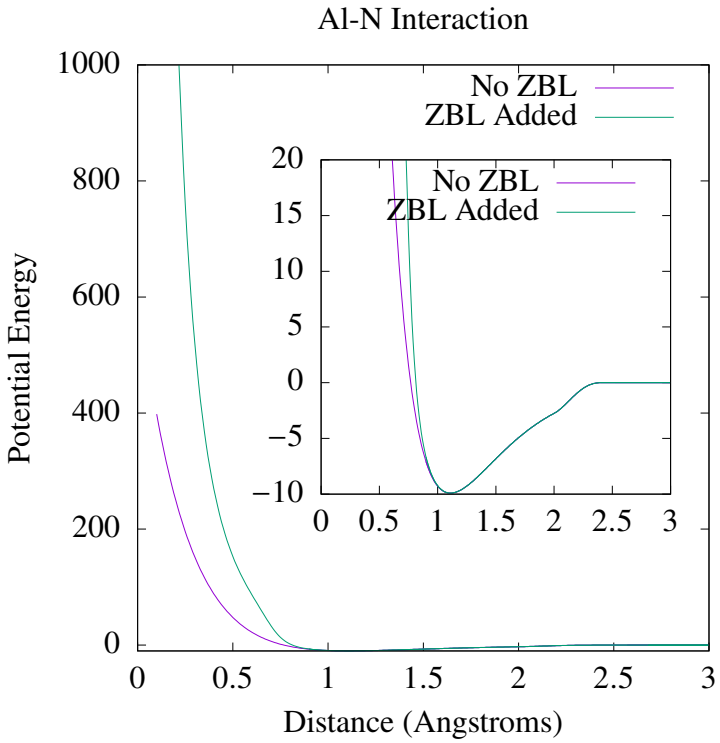

Figure 3.4. Tersoff-ZBL Potential for Nitrogen-Nitrogen

4. RESULTS

4.1. DEFECT FORMATION ENERGY

Table 4.1 summarizes our results for the defect formation energies for aluminum and nitrogen for both Tersoff and Buckingham potentials. We also compare these values to the displacement energies calculated by ab initio molecular dynamics.

Table 4.1. Defect Formation Energies in Aluminum Nitride

	Al Frenkel Pair (eV)	N Frenkel Pair (eV)	Antisite (eV)
Tersoff	15	8.1	21.5
Buckingham	14.84	13.76	30.83
Ab initio	19.6	10.9	20.3

In this table we see relative agreement between defect formation energies for both the Tersoff and Buckingham potential. Both potentials accurately recreate the relative energy costs relative to each other. That is, both potentials have the antisite as the most expensive, an aluminum Frenkel pair as the next expensive, and the nitrogen Frenkel pair as the easiest to create. The numbers for the Tersoff potential were of a generally lower energy compared to the ab initio work, aside from our antisite that had a very slightly higher formation energy. The defect formation energies of nitrogen were similar, but were off by greater values than the Tersoff energies. We expect the relative abundance of each of these defects to be proportional to these values. While the absolute values are differ by as much as 50%, it is important that the relative magnitude of the energies is more applicable for the simulations. That is, the nitrogen Frenkel pair has the lowest energy, followed by the aluminum Frenkel pair, and the antisite has the largest energy. This level of agreement in

defect formation energies is expected when working with classical potentials. However, on the basis of the defect formation energies alone, it is difficult to make a conclusion as to which is better for irradiation simulations.

4.2. DISPLACEMENT ENERGY

In these simulations, the simulation volume consisted of 17,280 atoms in a 48.25 $\mathring{A}$ x 66.86 $\mathring{A}$ x 61.81 $\mathring{A}$ box. We will calculate the displacement energy in two ways: Firstly along a pre-defined set of directions in order to compare to available ab initio results, and secondly along arbitrary directions to account for anisotropies of the system.

4.2.1. Crystallographic Directions. We firstly set the knock-on atom to test the displacement energy in deliberate directions. There directions were chosen to coincide with the work of Xi et al. [34] as a measure of verification for potentials employed in this work. These directions are given as $[0001]$, $[000\bar{1}]$, $[11\bar{2}0]$, $[\bar{1}\bar{1}20]$, and $[\bar{1}010]$. The results of our displacement energies are given in Table 4.2 and compared to those calculated by Xi et al.

Table 4.2. The Displacement Energies in eV along specific crystallographic directions

		$[0001]$	$[000\bar{1}]$	$[11\bar{2}0]$	$[\bar{1}\bar{1}20]$	$[\bar{1}010]$
Tersoff	Al	112	101	31	51	26
	N	85	118	24	21	29
Buckingham	Al	210	210	160	220	80
	N	280	320	230	260	120
DFT	Al	>145	123	58	52	120
	N	122	112	44	19	20

Our results for the Tersoff displacement energy is generally in much better agreement with ab initio calculations than those for Buckingham potential. The only result with a significant difference is the displacement of the aluminum atom in the $[\bar{1}010]$ direction. Otherwise, these numbers are in good agreement for the justification of the use of this potential.

The Buckingham potential on the other hand, does not seem to have very good agreement with the ab initio calculations anywhere. Compounded with the results of the Defect Formation Energy, our results for the displaycement energies suggest that this particular potential is a poor fit for this situation. Because of this ill-fit we deem to not continue forward with the consideration of this potential, and will instead focus on the application of the Tersoff potential to irradiation cascade simulations.

Further of note is the very striking anisotropy of the energies. The displacement energy of the system has a large correlation with the oncoming direction of the PKA particle. In the experimental setting, this direction is impossible to control, as the rebound atoms will have all possible directions within the crystal. In accord with this, it's it's important to calculate the displacement energy over arbitrary directions, and not only these specific few. Careful averaging can then be used for a better sense of the relevant values for this parameter.

4.2.2. Arbitrary Directions. For arbitrary directions, we allowed the incoming direction of the knock-on atom to vary to be in any direction. 176 random directions were considered for this averaging. We searched for displacement energies in the range of 10 eV to 150 eV, as this range cleanly encapsulates the range of values in the defect formation energy. The energies were studied in this range in discrete steps of 10 eV.

In order to fully understand the dynamics of the system, each arbitrary direction was also run from 20 different initial configurations. This allows us a more comprehensive view of the likelihood each energy will produce a lasting defect.

For all 20 different initial configurations, the simulation was run at an NVE thermostat with a timestep of $2.5 * 10^{-4}$ ps for 2 ps. At the end of the simulation the energy of the system was minimized .

The presence of a defect in this system was determined by comparing it's final potential energy to the potential energy of an idealized system. Since the energy minimization only finds local minima, it will not anneal out any defects and thus leave the system with a different potential energy. If the simulated system had a total energy greater than the reference system by 1 eV[1] a defect was declared found.

The percent of systems to have acquired a defect is then counted, and we thus say that there is a percent chance to form a defect at that energy in that direction. The defect formation energy of this direction was then counted as the first energy where the percent to create a defect was greater than 50 percent.

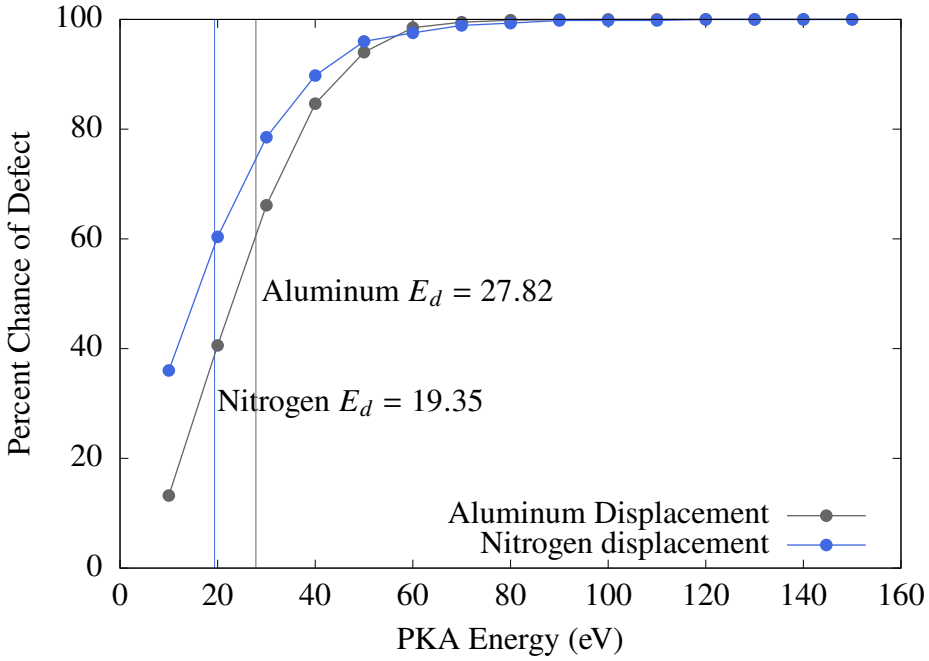

Figure 4.1. Percent chance of creating a defect for an arbitrary direction

[1] 1 eV is a buffer so slight differences in minimization won't be false positives for defects.

In Figure 4.1 we have plotted the relationship between the energy of the primary knock-on atom vs the chance of it to produce a defect. As we increase the knock-on energy of the atom, both the nitrogen and aluminum curve start out with a rougly linear dependence on energy. However, as they near the highest energies they begin to top out as there are very few directions that *won't* create an interstitial.

Given the results of the defect formation calculations, the values of the displacement energy in Figure 4.1 may seem surprising at a first glance. The threshold displacement energy of aluminum and nitrogen are smaller than *all* of the ones that were calculated along specific crystallographic directions.

But upon further consideration of these directions, this lower energy is not as unpredictable. This can mostly be understood since the crystallographic directions sent the atom directly into neighboring atoms, with no variance in direction. These arbitrary directions however, can and will "glance" off of it's nearest neighbors and be sent into areas of the crystal with fewer neighbors[2]. This further enforces the need for the averaging over arbitrary directions, as these arbitrary directions can find yet smaller displacement energies.

He et al. calculated the displacement energy of gallium nitride, which we can compare to[3]. They calculated the displacement energy as about 52 eV. This reported number is higher by a significant margin compared to our results. This then suggests that defects are easier to create in aluminum nitride.

4.3. CASCADE PRODUCTIONS

Summarized in Table 4.3 are our results for the main production cascade.

[2]In extreme cases, the atom can be sent in a direction where it passes through the gaps in the periodic structure and thus find a very low displacement energy. This is known as the *channeling effect.*

[3]He et al. displacements were clustered around the $[000\bar{1}]$ direction, and were not averaged over all 3D space. This does invite a more careful comparison, as we already know displacement direction is important from 4.2.1

Table 4.3. Breakdown of various defects by type and species

		Knock on energy (eV)									
		1000	2000	3000	4000	5000	6000	7000	8000	9000	10000
Al	Average	3.0	7.0	9.4	12.8	18.9	21.4	22.0	28.6	29.4	32.2
	Max	16	33	36	41	73	71	83	92	104	107
N	Average	7.4	13.8	22.4	32.4	39.4	46.8	56.6	65.6	69.0	83.2
	Max	23	42	53	41	98	105	143	143	158	160
Antisites	Average	0.2	1.4	3.2	3.2	2.8	4	6.4	6.6	6.2	7.6
	Max	7	9	10	12	26	23	28	43	33	29

The most striking feature of this table is the relationship between the energy of the knock on atom and the amount of interstitials it will produce. As impact energy goes up, both the average interstitial count at the end of the run and the maximum interstitials encountered tend to increase.

Note that the outliers to the above observation tend to occur in the maximum interstitial count. While this is somewhat curious, this result is not to be particularly unexpected. Since there is no statistical averaging applied to this attribute, it is the most likely to be affected by any statistical fluctuations. Further compounding this, we were not able to use Ovito to analyze the structure at every timestep. This is due to the size and amount of data to analyze growing very quickly as you try to analyze the structure for finer timesteps. Because of this, the listed maximum here is only compared to the timesteps we analyzed, and is likely not the ”true” maximum (and is only exacerbated at higher energy values).

Figure 4.2 shows the maximum counts of each defect at each energy. The solid lines represent the maximum defect counts from our simulations, and the dashed lines are the theoretical predictions from the NRT model for the respective atom type[4].

[4]As discussed,the NRT model normally incorporates the loss of energy available for the cascade via electronic stopping. The dashed lines do not have this consideration, and is the knock-on energy of each atom

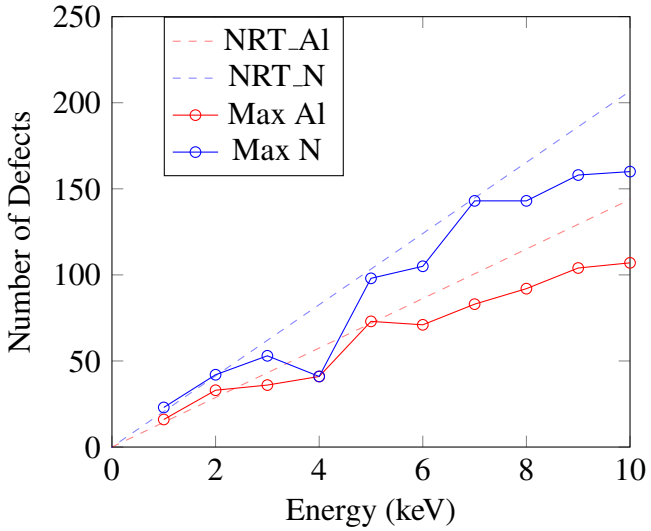

Figure 4.2. Maximum Number of Defects

The only time a decrease in an average quantity occurs after an increase an energy is in the average antisite count from 4000 eV to 5000 eV, and from 8000 eV to 9000 eV. While we expect this to be an anomaly of the statistical averaging, rather an an inherent feature to the system, it suggests the possibility of more analysis to determine if this is the case.

Figure 4.3 compares the average number of each defect at the end of the simulation. The NRT model lines in comparison were generated by finding a best fit factor $\Phi < 1$ to multiply the NRT model by. This was done with a simple least squares regression $N_{end} = \Phi N_{max}$ where N_{end} is the number of defects present at the end of each run, N_{max} is the maximum number of defects, and Φ was the factor solved for.

As expected from the results in Section 5.1, the relative magnitude of defects goes proportionally to their defect formation energy. Nitrogen interstitials, being the least energetically costly, are on average the most prevalent at the end of each simulation. And at each energy step they also have the highest count present except for 4000 eV, where at some point in an irradiation cascade there were 41 of both interstitials present (not necessarily at the same time). Antisites being the most energetically costly defects are seen very rarely in comparison.

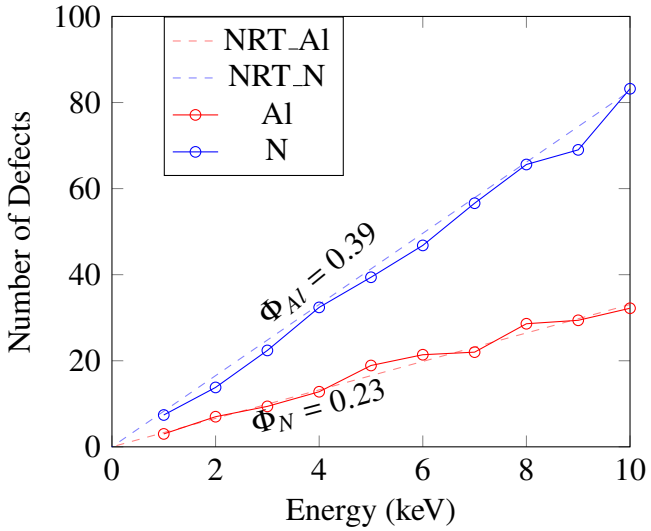

Figure 4.3. Number of Defects at $t = 2$ ps

Table 4.4. Comparison of Frenkel pairs

	Frenkel Pairs at end of run
AlN	118.6 ± 6.73
GaN	51.30 ± 1.15

The work of He. et. al computed similarly the amount of defects after an irradiation event. Their work was done with respect GaN, and their simulations were run to 12.4 ps. We compare the results of our work in Table 4.4. Compared to their work, aluminum nitrogen appears to be less resistant to persistent Frenkel Pairs over time. Specifically, the recombination percentage of aluminum-nitrogen wurtzite is much lower despite having a lower maximum number of defects present. This suggests that while it is more resistant to initial irradiation, these defects anneal out much less efficiently compared to gallium nitrogen.

5. CONCLUSIONS

In this work we have discussed the use of molecular dynamics as a method of physics experimentation. Core features of molecular dynamics simulations such as thermostats, equilibration, and potentials were explained in order to establish a conceptual understanding. A description of the knock-on atom technique was given, and how it allows a simulation of an irradiated particle and subsequent defect cascadel

In preparation for their use in the simulations, there was special attention paid to the Buckingham pairwise potential and the Tersoff bond-order potential. An overview of the core features of these potentials were given, as well as the parameters previous works had used to allow it to describe aluminum nitride. We then applied this with the LAMMPS package to investigate various facets of defect productions in w-AlN

We applied both the pairwise Buckingham potential and Tersoff potential to measure defect production in aluminum nitride in 3 facets: defect formation energy, displacement energy, and cascade production from an irradiated particle. All of these properties were studied in relation to the energy of the knock-on atom, and the direct effects of this energy on defect production.

In order to judge the quality of the potentials as applied to our simulation, we first calculated the defect formation energy of isolated Frenkel pairs and compared our results to ab initio work done previously. As a first test, both the Tersoff and Buckingham potential compared favorably to previous results. Both potentials recreated defect formation energies similar to ab initio works.

To further test these potentials for applicability to the simulations, we also calculated the displacement energy along certain crystallographic directions, and again compared these results to previous ab initios calculations. From these results, we concluded that the Buckingham potential was not as well-suited for irradiation cascades as the Tersoff potential. So in subsequent simulations, we only modelled the Tersoff potential.

With the Tersoff potential chosen to be the more accurate description, the directions along which we searched for the displacement energy were allowed to vary to any direction. This new value was averaged to obtain displacement energies for both aluminum and nitrogen atoms. The value was averaged with respect to all directions. Consistent with our results in the defect formation energy, we saw aluminum as having a higher displacement energy when compared to nitrogen. Both of these values were lower when compared to similar calculations done for gallium nitride.

Lasty, the irradiation cascade of the supercell under the Tersoff potential was simulated. We observed again the strict dependence of the number of defects produced related to the knock on energy of the atom. The number of persistent Frenkel pairs created was rougly linear to the knock-on energy. In addition, the relative abundance of each species of interstitial was similar to their defect formation energy as predicted. This meant nitrogen interstitials were the most abundant, followed by aluminum interstitials, with antisites being rare in comparison.

APPENDIX

CODE EXAMPLES

The following is the LAMMPS input script that was used to create equilibrated systems. Lines *2-4* define basic physical properties of our systems. Lines *12-23* create a custom lattice with which to put atoms on to create a wurtzite cell. Lines *26-34* define which atoms go on which lattice site. Lines *37-40* create basic physical parameter for our 2 atom types. Atom one has the physical values of aluminum, and atom 2 has the values corresponding to nitrogen. Lines *43-44* create fixes to control our simulation. Lines *46-47* tell LAMMPS to use the Tersoff potential, and where to find the parameter list. Lines *53-57* concern tracking of observables during the simulation, and how they are printed to the output file. Lines *59-70* run the simulation, and tell LAMMPS how often to write out the structure, and to create a file that can be read for a new simulation.

Equilibration Script

```
1  # Basic setup
2  units metal # Select units
3  timestep .001 # Timestep in ps
4  atom_style charge
5
6  variable latt equal  3.11
7  variable a equal  1.0
8  variable b equal  sqrt(3.0)
9  variable c equal  4.98/3.11
10
11 # Create the primitive lattice
12 lattice custom     ${latt} &
```

```
        a1        $a        0.0       0.0       &
        a2        0.0       $b        0.0       &
        a3        0.0       0.0       $c        &
        basis     0.0       0.0       0.0       &
        basis     0.0 0.0       0.7       &
        basis     0.5 0.5       0.7       &
        basis     0.5 0.175     0.25      &
        basis     0.5       0.5       0.0       &
        basis     0.5       0.175     0.55      &
        basis     0.0       0.7       0.55      &
        basis     0.0       0.7       0.25
region myreg block 0 1 0 1 0 1
create_box          2 myreg
create_atoms        1 box           &
          basis     1     2   &
    basis     2     1   &
    basis     3     1   &
    basis     4     1   &
    basis     5     2   &
    basis     6     2   &
    basis     7     2   &
    basis     8     1

# Insert Aluminum and Nitrogen Mass
mass 1 26.981539
mass 2 14.0067
set type 1 charge 2.0
```

```
set type 2 charge -2.00
#make a run with these as +2 and -2
compute 2 all temp
fix 1 all npt temp 300.0 300.0 1.0 iso 0.0 0.0 1.0
fix 2 all ave/time 100 5 1000 c_thermo_temp c_thermo_press

pair_style tersoff/zbl
pair_coeff * * ../AlN.tersoff.zbl Al N

replicate 50 40 40

# Outputs
# Computes all kinetic energies and finds the maximum
compute KE all ke/atom
compute maxKE all reduce max c_KE
# Configure the information printout
thermo 100
thermo_style custom ke c_maxKE pe etotal step temp

# Run the Equilibrium script
# Dumps must be defined before run
dump myDump all atom 3000 MinRun20k.struct
# Start from a minimized lattice
minimize 1.0e-7 1.0e-7 10000 10000
# Give atoms a random velocity
velocity all create 300 509
# Run
```

```
run 20000

# Write restart file for Cascade Simulations
write_restart minRun20k.equil
```

The following code was run to analyze LAMMPS structure files for defects. Lines *1-6* import the OVITO module for Python to be used. Line *8* starts the code by importing the structures that have been dumped from LAMMPS. Lines *10-13* uses OVITO's Wigner-Seitz Analysis function to analyze the structure for defects. Lines *17-19* append functions that further break down the Wigner-Seitz analysis into counts of the individual defect types. The loop at line *32* starts looping over all realizations of the simulations. The inner loop at line *42* analyzes each individual simulation through each timestep. The final lines print out the results of the analyzation.

Python analysis for defects

```
#!/opt/homebrew/bin/python3.10
from ovito.io import *
from ovito.data import *
from ovito.modifiers import *
from ovito.pipeline import *
from Inter import *

pipeline = import_file("1/Trajectories/Run*.struct")
# Perform Wigner-Seitz analysis:
ws = WignerSeitzAnalysisModifier(
    per_type_occupancies = True,
    affine_mapping =
    ReferenceConfigurationModifier.AffineMapping.ToReference)
pipeline.modifiers.append(ws)
```

```
15
16
17  # Insert Python modifiers into the data pipeline.
18  pipeline.modifiers.append(AlInter)
19  pipeline.modifiers.append(NInter)
20  pipeline.modifiers.append(AlAnti)
21
22  # Arrays to hold end of run counts. These will be averaged
23  AlAvg=[]
24  NAvg=[]
25  AntiAvg=[]
26
27  # Maximum counts for each type of defect are initialized to 0
28  AlMax=0
29  NMax=0
30  AntiMax=0
31
32  # Main loop that goes through all runs
33  for i in range (1,6):
34      # Gets structure data from LAMMPS files
35      pipeline.source.load(str(i)+"/Trajectories/Run*.struct")
36
37      print("Evaulating series",i)
38
39      # Initialize Arrays to hold time series
40      AlTime =    []
41      NTime =     []
```

```
    AntiTime = []
    for frame in range(pipeline.source.num_frames):
        # Let ovito calculate
        data=pipeline.compute(frame)
        # Get count of Al Interstitials
        AlCount = data.attributes['Al_Interstitials']
        # Add To Time series
        AlTime.append(AlCount)
        # Get count of N Interstitials
        NCount = data.attributes['N_Interstitials']
        # Add to time series
        NTime.append(NCount)
        # Get Count of Antisites
        AntiCount = data.attributes['Antisites']
        # Add to time series
        AntiTime.append(AntiCount)

    # Print Statistics of Individual run
    print("Max Al: ",max(AlTime),
          "| Max N: ",max(NTime),
          "| Max Anti: ",max(AntiTime))
    print("Ending Al: ",AlTime[-1],
          "Ending N: ",NTime[-1],
          "Ending Anti: ",AntiTime[-1])
    # Add ending counts to our Averaging arrays
    AlAvg.append(AlTime[-1])
    NAvg.append(NTime[-1])
```

```
69      AntiAvg.append(AntiTime[-1])
70      # Update our maximum counts if any are greater
71      AlMax=max(AlMax,max(AlTime))
72      NMax=max(NMax,max(NTime))
73      AntiMax=max(AntiMax,max(AntiTime))
74
75  print("Average endings are: ",np.average(AlAvg),
76                                 np.average(NAvg),
77                                 np.average(AntiAvg))
78  print("The maximums for each were: ",AlMax,NMax,AntiMax)
```

The following code is the *Inter* file that was imported. It contains the functions that detect and count the number and type of defects.

```
"Functions for Analysis
1   import numpy as np
2
3   ### Modifier that counts total Aluminum Interstitials
4   def AlInter(frame,data):
5
6       # Get occupancy data
7       occupancies = data.particles['Occupancy']
8
9       # And initial site types
10      site_type=data.particles['Particle Type']
11
12      # Get total occupancy of each site
13      total_occupancy = np.sum(occupancies,axis=1)
14
```

```
15      #Set up a particles selection by creating property 'Selection'
16      selection = data.particles_.create_property('Selection')
17
18      #Count all interstitials
19      # Aluminum interstitial is
20      # An Al Site with 2 Al atoms
21      # Or a N site with 1 Al atom and 1 N atom
22      selection[...] = (
23      (site_type==1) & (occupancies[:,0]==2))
24      | ((site_type==2) & (occupancies[:,0]==1) & (occupancies[:,1]==1))
25
26      # And make it a global property
27      data.attributes['Al_Interstitials']= np.count_nonzero(selection)
28
29  ### Modifier that counts total Nitrogen Interstitials
30  def NInter(frame,data):
31
32      # Get occupancy data
33      occupancies = data.particles['Occupancy']
34
35      # And initial site types
36      site_type=data.particles['Particle Type']
37
38      # Get total occupancy of each site
39      total_occupancy = np.sum(occupancies,axis=1)
40
41      #Set up a particles selection by creating property 'Selection'
```

```
42      selection = data.particles_.create_property('Selection')
43
44      # Count all interstitials
45      # Nitrogen interstitial is an N Site with 2 N atoms
46      # Or a Al site with 1 Al atom and 1 N atom
47      selection[...] =
48      ((site_type==2) & (occupancies[:,1]==2)) |
49      ((site_type==1) & (occupancies[:,0]==1) & (occupancies[:,1]==1))
50
51      # And make it a global property
52      data.attributes['N_Interstitials']= np.count_nonzero(selection)
53
54  def AlAnti(frame,data):
55
56      # Get all occupancies
57      occupancies = data.particles['Occupancy']
58
59      #And their reference site types
60      site_type=data.particles['Particle Type']
61
62      # Get total amount of atoms on each site
63      total_occupancy = np.sum(occupancies,axis=1)
64
65      # Create a property so we can select particles
66      selection = data.particles_.create_property('Selection')
67
68      # Count all Antisites
```

```
    selection[...]=
    (total_occupancy==1) &
    (((site_type==1)
     & (occupancies[:,1]==1))
    | ((site_type==2)
     & (occupancies[:,0]==1)))

    # Make it an outputtable property
    data.attributes['Antisites'] = np.count_nonzero(selection)
```

The following is the bash script that was run to calculate the percent chance of forming defects.

Aribtrary Displacement

```
#!/bin/sh
source ../getVelocity.sh
source ../normalizedDirection.sh

#Start by choosing a random direction
getDirection #Returns a 3d unit vector

###REFERENCE RUN
sed "s/Vx/0/g;
     s/Vy/0/g;
     s/Vz/0/g;
     s/evGrowthI/evGrowth0/g;
     s/Seed.eq/15000.eq/g;" \
     thatsalatticeimsure_50 > thatsalatticeimsure_50.curr
echo "Run LAMMPS"
```

```
mpirun lmp_mpi < thatsalatticeimsure_50.curr > "out_0.dat"
echo "Extract data from LAMMPS"
E_ref=‘tac "out_0.dat"
      | grep -A 1 Loop -m1
      | tail -n 1
      |awk '{print $3}'‘

#Iterate between 0 and 150 in increments of 10 ev
for i in {20..400..20}
do
   #Get knock on velocity for current eV
   getVelocity "2" "$i"

   #Give the knock on particle that velocity
   x_vel=‘echo "scale=10;$x_dir*$velocityTarget"|bc‘
   y_vel=‘echo "scale=10;$y_dir*$velocityTarget"|bc‘
   z_vel=‘echo "scale=10;$z_dir*$velocityTarget"|bc‘
   echo "$x_vel $y_vel $z_vel"
   displaceCount='0'
   for seed in {16000..35000..1000}
   do
      sed "s/Vx/$x_vel/g;
           s/Vy/$y_vel/g;
           s/Vz/$z_vel/g;
           s/evGrowthI/evGrowth$i/g;
           s/Seed/$seed/g;"
           thatsalatticeimsure_50 > thatsalatticeimsure_50.curr
```

```
43
44          mpirun lmp_mpi < thatsalatticeimsure_50.curr > "out_$i.dat"
45          E_cur=`tac "out_$i.dat"
46                  | grep -A 1 Loop -m1
47                  | tail -n 1
48                  |awk '{print $3}'`
49
50          if (( $(echo "$E_cur -7.0 > $E_ref"|bc -l) ))
51          then
52             ((displaceCount++))
53             echo "Displacement found at $i !"
54          else
55             echo "None found at $i !"
56          fi
57      done
58      echo $displaceCount
59      percentChance=`echo "scale=3;($displaceCount/20)*100"|bc`
60      echo "The percent chance of defect is $percentChance at $i eV"
61
62      #Write important variables out to seperate file
63      printf "%12s |%12s |%12s |%5s \n"
64             "$x_dir" "$y_dir" "$z_dir" "$percentChance"
65             >> /path/to/dir/"${i}.out"
66  done
67  exit
```

REFERENCES

[1] J. L. Rempe, D. L. Knudson, J. E. Daw, T. C. Unruh, B. M. Chase, K. L. Davis, A. J. Palmer, and R. S. Schley. Advanced in-pile instrumentation for material and test reactors. In *2013 3rd International Conference on Advancements in Nuclear Instrumentation, Measurement Methods and their Applications (ANIMMA)*, pages 1–11, 2013. doi: 10.1109/ANIMMA.2013.6728013.

[2] Zhengbao Yang, Shengxi Zhou, Jean Zu, and Daniel Inman. High-performance piezoelectric energy harvesters and their applications. *Joule*, 2(4):642–697, April 2018. doi: 10.1016/j.joule.2018.03.011. URL https://doi.org/10.1016/j.joule.2018.03.011.

[3] A. Kozlovskiy, I. Kenzhina, K. Dukenbayev, and M. Zdorovets. Influence of he-ion irradiation of ceramic AlN. *Vacuum*, 163: 45–51, May 2019. doi: 10.1016/j.vacuum.2019.02.005. URL https://doi.org/10.1016/j.vacuum.2019.02.005.

[4] K. Dukenbayev, A. Kozlovskiy, Z. A. Alyamova, T. Gladkikh, I. Kenzhina, and M. Zdorovets. The investigation of various type irradiation effects on aluminum nitride ceramic. *Journal of Materials Science: Materials in Electronics*, 30(9):8777–8787, March 2019. doi: 10.1007/s10854-019-01202-6. URL https://doi.org/10.1007/s10854-019-01202-6.

[5] S. Jublot-Leclerc, F. Pallier, L. Delauche, and A. Declémy. Temperature dependent he-enhanced damage and strain in he-implanted AlN. *Journal of Nuclear Materials*, 523:369–377, September 2019. doi: 10.1016/j.jnucmat.2019.06.025. URL https://doi.org/10.1016/j.jnucmat.2019.06.025.

[6] S. Jublot-Leclerc, G. Bouhali, F. Pallier, and A. Declémy. Temperature dependence of elastic strain and damage build-up in he implanted AlN. *Journal of the European Ceramic Society*, 41(1):259–267, January 2021. doi: 10.1016/j.jeurceramsoc.2020.08.010. URL https://doi.org/10.1016/j.jeurceramsoc.2020.08.010.

[7] S. O. Kucheyev, J. S. Williams, J. Zou, C. Jagadish, M. Pophristic, S. Guo, I. T. Ferguson, and M. O. Manasreh. Ion-beam-produced damage and its stability in AlN films. *Journal of Applied Physics*, 92(7):3554–3558, October 2002. doi: 10.1063/1.1501746. URL https://doi.org/10.1063/1.1501746.

[8] W Jiang, I-T Bae, and W J Weber. Disordering and dopant behaviour in au+-ion-irradiated aln. *Journal of Physics: Condensed Matter*, 19 (35):356207, aug 2007. doi: 10.1088/0953-8984/19/35/356207. URL https://dx.doi.org/10.1088/0953-8984/19/35/356207.

[9] M. Sall, I. Monnet, C. Grygiel, B. Ban d'Etat, H. Lebius, S. Leclerc, and E. Balanzat. Synergy between electronic and nuclear energy losses for color center creation in AlN. *EPL (Europhysics Letters)*, 102(2):26002, April 2013. doi: 10.1209/0295-5075/102/26002. URL https://doi.org/10.1209/0295-5075/102/26002.

[10] A Kozlovskiy, K Dukenbayev, I Ivanov, S Kozin, V Aleksandrenko, A Kurakhmedov, E Sambaev, I Kenzhina, D Tosi, V Loginov, and M Zdorovets. Investigation of the influence of irradiation with fe+7 ions on structural properties of aln ceramics. *Materials Research Express*, 5(6):065502, jun 2018. doi: 10.1088/2053-1591/aac7ba. URL https://dx.doi.org/10.1088/2053-1591/aac7ba.

[11] Toyohiko Yano and Takayoshi Iseki. A hrem study of neutron-irradiation-induced dislocations in aluminium nitride. *Philosophical Magazine Letters*, 62(2):83–87, August 1990. doi: 10.1080/09500839008203743. URL https://doi.org/10.1080/09500839008203743.

[12] Q. Hu, S. Tanaka, T. Yoneoka, and V. Grismanovs. In-situ luminescence measurement for aln ceramics under reactor irradiation. *Radiation Effects and Defects in Solids*, 147(4):283–292, 1999. doi: 10.1080/10420159908226996. URL https://doi.org/10.1080/10420159908226996.

[13] T Yano, K Ichikawa, M Akiyoshi, and Y Tachi. Neutron irradiation damage in aluminum oxide and nitride ceramics up to a fluence of. *Journal of Nuclear Materials*, 283-287:947–951, December 2000. doi: 10.1016/s0022-3115(00)00092-1. URL https://doi.org/10.1016/s0022-3115(00)00092-1.

[14] Stephen J. Pearton, Richard Deist, Fan Ren, Lu Liu, Alexander Y. Polyakov, and Jihyun Kim. Review of radiation damage in GaN-based materials and devices. *Journal of Vacuum Science and Technology A*, 31(5), 04 2013. ISSN 0734-2101. doi: 10.1116/1.4799504. URL https://doi.org/10.1116/1.4799504. 050801.

[15] Kai Nordlund, Steven J. Zinkle, Andrea E. Sand, Fredric Granberg, Robert S. Averback, Roger E. Stoller, Tomoaki Suzudo, Lorenzo Malerba, Florian Banhart, William J. Weber, Francois Willaime, Sergei L. Dudarev, and David Simeone. Primary radiation damage: A review of current understanding and models. *Journal of Nuclear Materials*, 512:450–479, December 2018. doi: 10.1016/j.jnucmat.2018.10.027. URL https://doi.org/10.1016/j.jnucmat.2018.10.027.

[16] Jianqi Xi, Bin Liu, Yanwen Zhang, and William J. Weber. Ab initio molecular dynamics simulations of AlN responding to low energy particle radiation. *Journal of Applied Physics*, 123(4), 01 2018. ISSN 0021-8979. doi: 10.1063/1.5009750. URL https://doi.org/10.1063/1.5009750. 045904.

[17] He, Huan, et al. Primary damage of 10 keV Ga PKA in bulk GaN material under different temperatures. *Nuclear Engineering and Technology*, 52 (7):1537–1544, 2020. doi: https://doi.org/10.1016/j.net.2019.12.027. URL https://www.sciencedirect.com/science/article/pii/S1738573319306679.

[18] J. Nord, K. Nordlund, and J. Keinonen. Molecular dynamics study of damage accumulation in gan during ion beam irradiation. *Phys. Rev. B*, 68:184104, 11 2003. doi: 10.1103/PhysRevB.68.184104. URL https://link.aps.org/doi/10.1103/PhysRevB.68.184104.

[19] A. P. Thompson, H. M. Aktulga, R. Berger, D. S. Bolintineanu, W. M. Brown, P. S. Crozier, P. J. in 't Veld, A. Kohlmeyer, S. G. Moore, T. D. Nguyen, R. Shan, M. J. Stevens, J. Tranchida, C. Trott, and S. J. Plimpton. LAMMPS - a flexible simulation tool for particle-based materials modeling at the atomic, meso, and continuum scales. *Comp. Phys. Comm.*, 271:108171, 2022. doi: 10.1016/j.cpc.2021.108171.

[20] Alexander Stukowski. Visualization and analysis of atomistic simulation data with OVITO-the Open Visualization Tool. *MODELLING AND SIMULATION IN MATERIALS SCIENCE AND ENGINEERING*, 18(1), JAN 2010. ISSN 0965-0393. doi: 10.1088/0965-0393/18/1/015012.

[21] Kai Nordlund, Steven J Zinkle, Andrea E Sand, Fredric Granberg, Robert S Averback, Roger E Stoller, Tomoaki Suzudo, Lorenzo Malerba, Florian Banhart, William J Weber, et al. Primary radiation damage: A review of current understanding and models. *Journal of Nuclear Materials*, 512:450–479, 2018.

[22] G H Kinchin and R S Pease. The displacement of atoms in solids by radiation. *Reports on Progress in Physics*, 18(1):1, jan 1955. doi: 10.1088/0034-4885/18/1/301. URL https://dx.doi.org/10.1088/0034-4885/18/1/301.

[23] M.J. Norgett, M.T. Robinson, and I.M. Torrens. A proposed method of calculating displacement dose rates. *Nuclear Engineering and Design*, 33(1):50–54, 1975. ISSN 0029-5493. doi: https://doi.org/10.1016/0029-5493(75)90035-7. URL https://www.sciencedirect.com/science/article/pii/0029549375900357.

[24] Priya Vashishta, Rajiv K. Kalia, Aiichiro Nakano, José Pedro Rino, Collaboratory for Advanced Computing, and Simulations. Interaction potential for aluminum nitride: A molecular dynamics study of mechanical and thermal properties of crystalline and amorphous aluminum nitride. *Journal of Applied Physics*, 109(3), 02 2011. ISSN 0021-8979. doi: 10.1063/1.3525983. URL https://doi.org/10.1063/1.3525983. 033514.

[25] Henggao Xiang, Haitao Li, and Xianghe Peng. Comparison of different interatomic potentials for md simulations of aln. *Computational Materials Science*, 140:113–120, 2017. ISSN 0927-0256. doi: https://doi.org/10.1016/j.commatsci.2017.08.042. URL https://www.sciencedirect.com/science/article/pii/S0927025617304640.

[26] J. Tersoff. New empirical approach for the structure and energy of covalent systems. *Phys. Rev. B*, 37:6991–7000, Apr 1988. doi: 10.1103/PhysRevB.37.6991. URL https://link.aps.org/doi/10.1103/PhysRevB.37.6991.

[27] Mihir Tungare, Yunfeng Shi, Neeraj Tripathi, Puneet Suvarna, and Fatemeh (Shadi) Shahedipour-Sandvik. A tersoff-based interatomic potential for wurtzite aln. *physica status solidi (a)*, 208(7):1569–1572, 2011. doi: https://doi.org/10.1002/pssa.201001086. URL https://onlinelibrary.wiley.com/doi/abs/10.1002/pssa.201001086.

[28] P. Vashishta, Rajiv K. Kalia, José P. Rino, and Ingvar Ebbsjö. Interaction potential for sio_2: A molecular-dynamics study of structural correlations. *Phys. Rev. B*, 41:12197–12209, Jun 1990. doi: 10.1103/PhysRevB.41.12197. URL https://link.aps.org/doi/10.1103/PhysRevB.41.12197.

[29] Priya Vashishta, Rajiv K. Kalia, Aiichiro Nakano, and José Pedro Rino. Interaction potential for silicon carbide: A molecular dynamics study of elastic constants and vibrational density of states for crystalline and amorphous silicon carbide. *Journal of Applied Physics*, 101(10), 05 2007. ISSN 0021-8979. doi: 10.1063/1.2724570. URL https://doi.org/10.1063/1.2724570. 103515.

[30] Tao Liang, Tzu-Ray Shan, Yu-Ting Cheng, Bryce D. Devine, Mark Noordhoek, Yangzhong Li, Zhize Lu, Simon R. Phillpot, and Susan B. Sinnott. Classical atomistic simulations of surfaces and heterogeneous interfaces with the charge-optimized many body (comb) potentials. *Materials Science and Engineering: R: Reports*, 74(9):255–279, 2013. ISSN 0927-796X. doi: https://doi.org/10.1016/j.mser.2013.07.001. URL https://www.sciencedirect.com/science/article/pii/S0927796X13000612.

[31] J A Chisholm, D W Lewis, and P D Bristowe. Classical simulations of the properties of group-iii nitrides. *Journal of Physics: Condensed Matter*, 11(22):L235, jun 1999. doi: 10.1088/0953-8984/11/22/102. URL https://dx.doi.org/10.1088/0953-8984/11/22/102.

[32] James F. Ziegler and Jochen P. Biersack. *The Stopping and Range of Ions in Matter*, pages 93–129. Springer US, Boston, MA, 1985. ISBN 978-1-4615-8103-1. doi: 10.1007/978-1-4615-8103-1_3. URL https://doi.org/10.1007/978-1-4615-8103-1_3.

[33] Rushton, Michael. Potential Model Tabulation for Atomic Scale Simulation, 2021. URL https://atsimpotentials.readthedocs.io/en/latest/.

[34] Jianqi Xi, Bin Liu, Yanwen Zhang, and William J. Weber. Ab initio molecular dynamics simulations of AlN responding to low energy particle radiation. *Journal of Applied Physics*, 123(4), 01 2018. ISSN 0021-8979. doi: 10.1063/1.5009750. URL https://doi.org/10.1063/1.5009750. 045904.

VITA

Sean Thomas Anderson was born in Warrensburg, Missouri in 1999. After attendance in Warrensburg High School, he was accepted into the Missouri University of Science and Technology, and joined the Physics department after his first year of attendance. He was awarded a Bachelor's Degree of Physics in May 2022. He then returned to the Physics department and he received his masters degree from Missouri University of Science and Technology in Physics in July 2023.